

HIGH-EFFICIENCY DEVICE RESEARCH

N86-29374

COMPREHENSIVE SOLAR CELL MODELING AND
CORRELATION STUDIES

RESEARCH TRIANGLE INSTITUTE

M. L. Lamorte

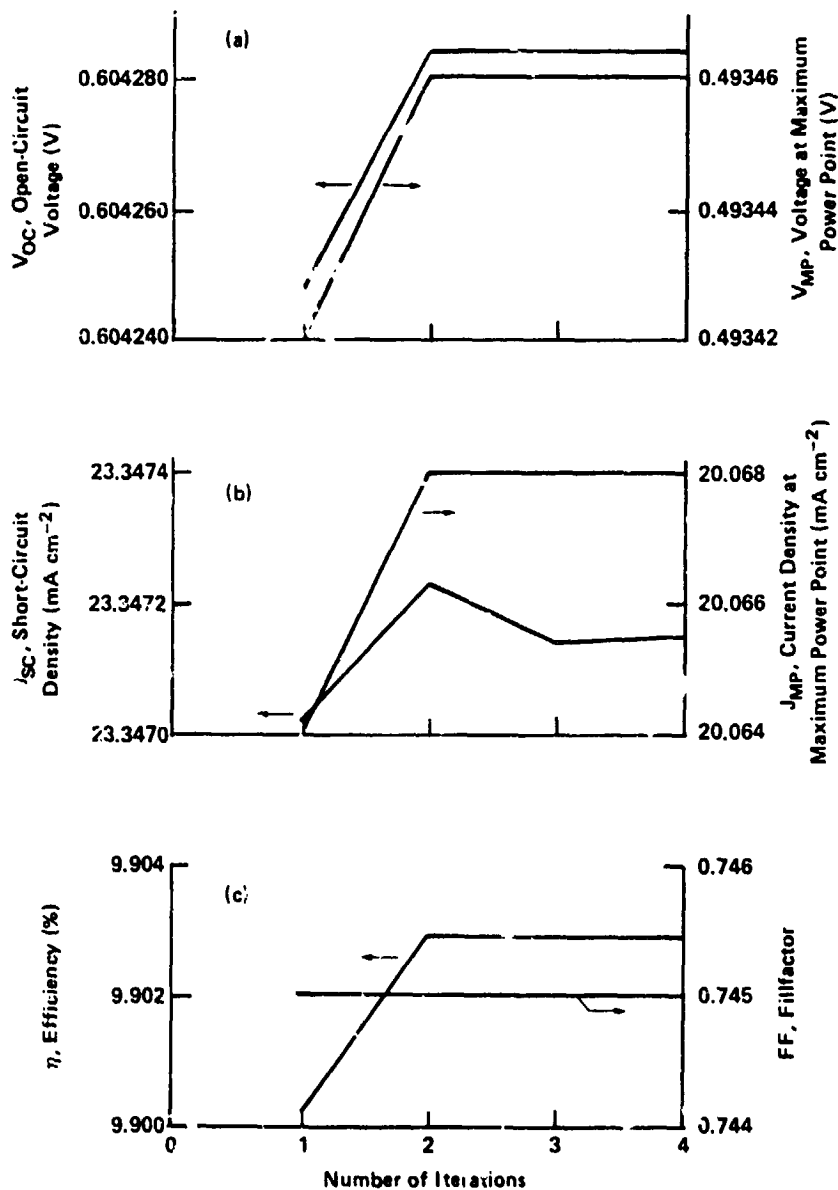


Figure 1. Solar cell terminal characteristics vs. number of iterations: (a) open-circuit and maximum power point voltages; (b) short-circuit and maximum power point current densities; and (c) efficiency and fillfactor. Twenty mesh points, twelve junction photovoltage simulations, and twenty V-I points were used.

HIGH-EFFICIENCY DEVICE RESEARCH

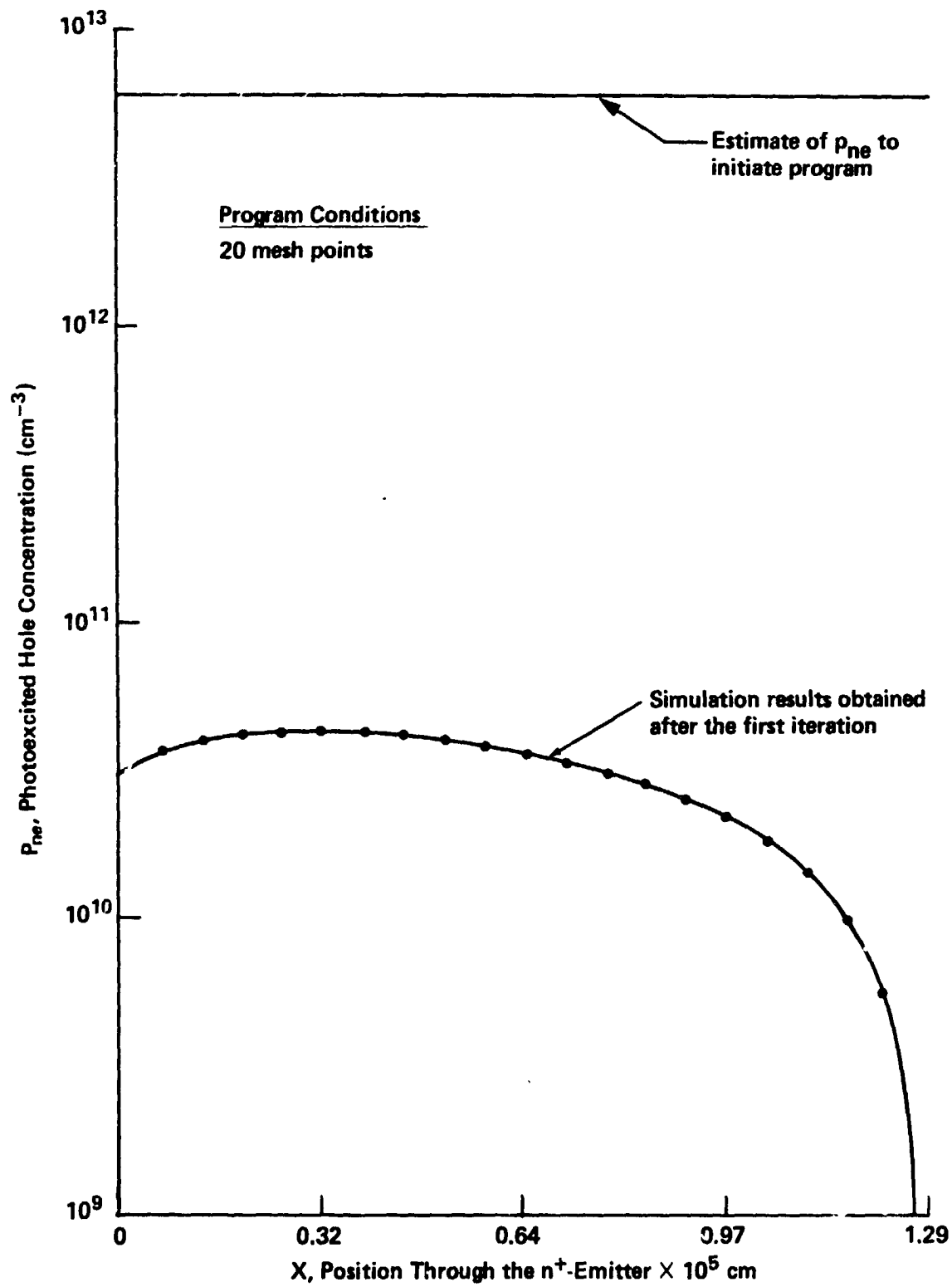


Figure 2. Photoexcited hole concentration vs. position in the n^+ -emitter.



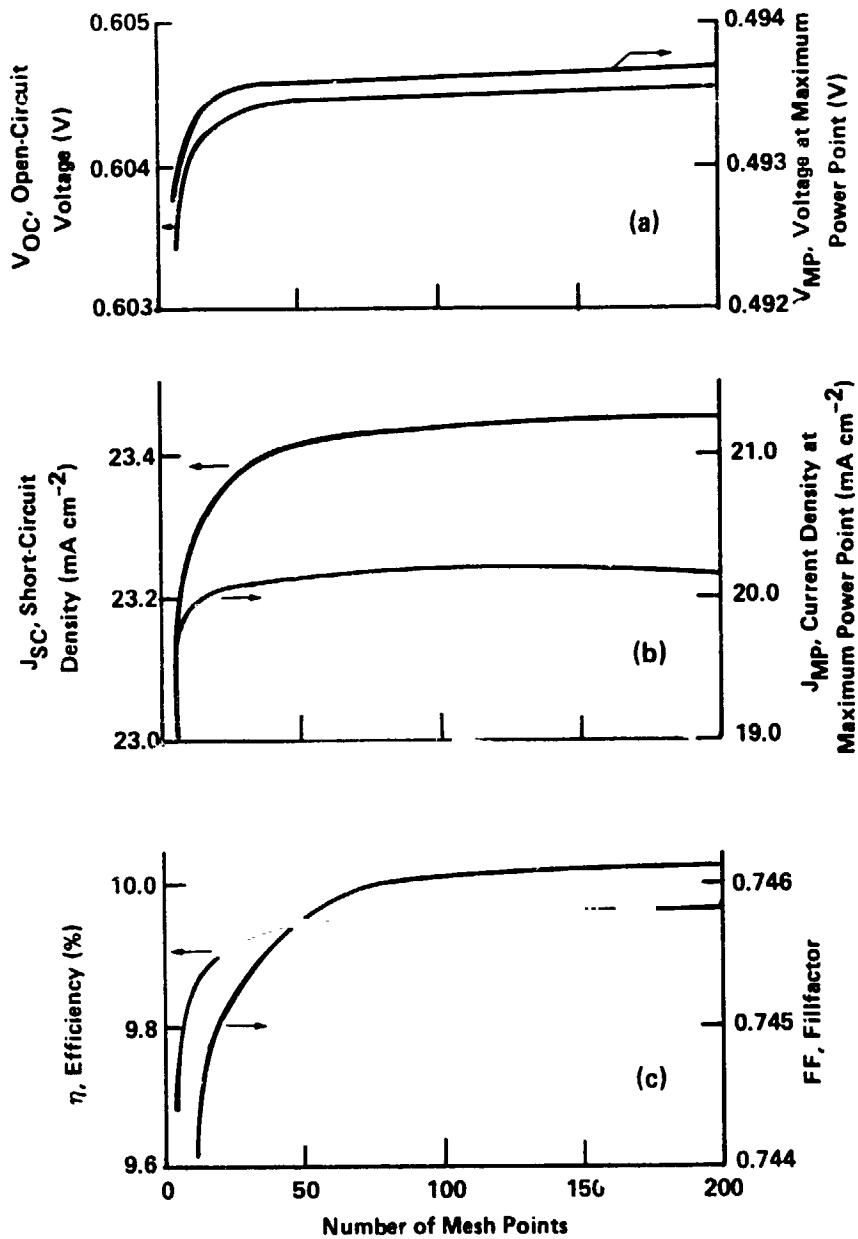


Figure 3. Solar cell terminal characteristics vs. number of mesh points: (a) open-circuit and maximum power point voltages; (b) short-circuit and maximum power point current densities; and (c) efficiency and fillfactor. Three iterations per mesh point, twelve junction photovoltage simulations, and twenty V-I points were used.

HIGH-EFFICIENCY DEVICE RESEARCH

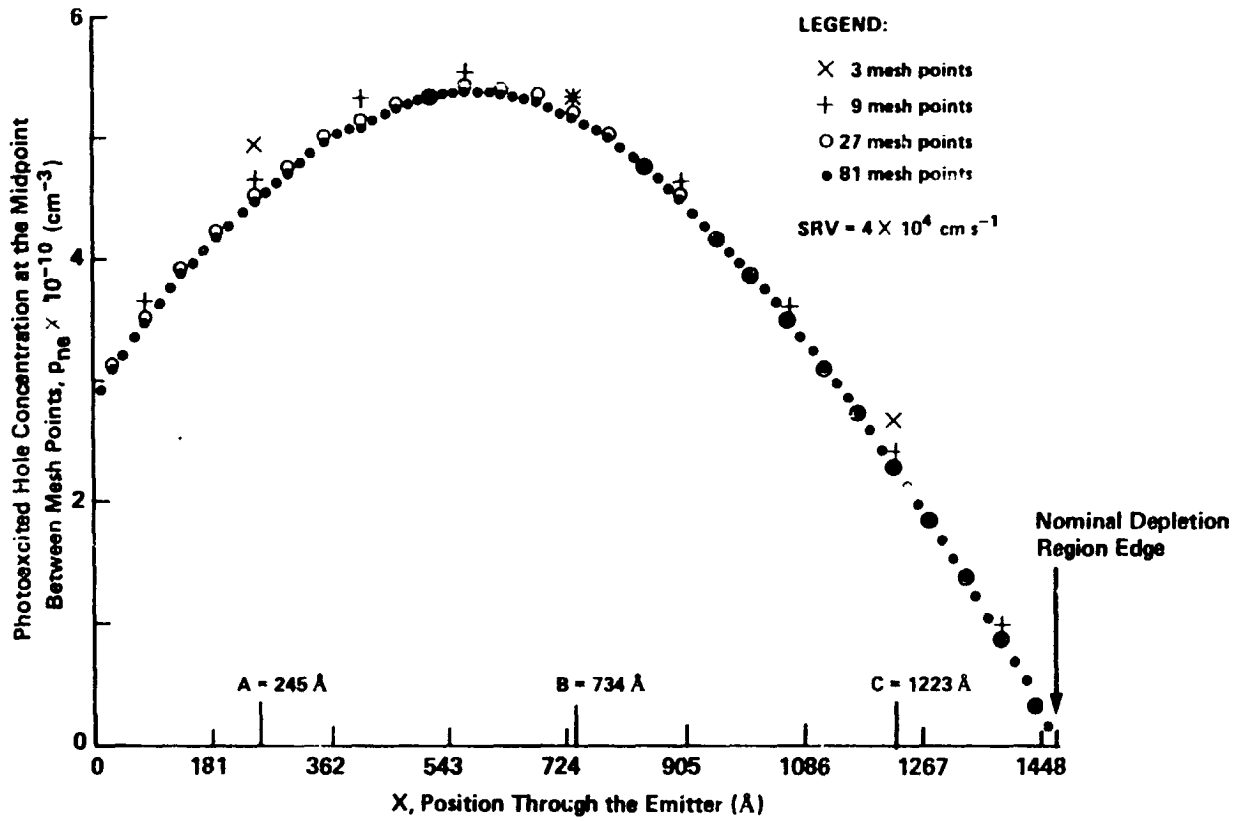


Figure 4. Photoexcited hole concentration calculated midway between mesh points in the n^+ -emitter for 3, 9, 27, and 81 mesh points under short-circuit conditions and for three iterations per mesh point.



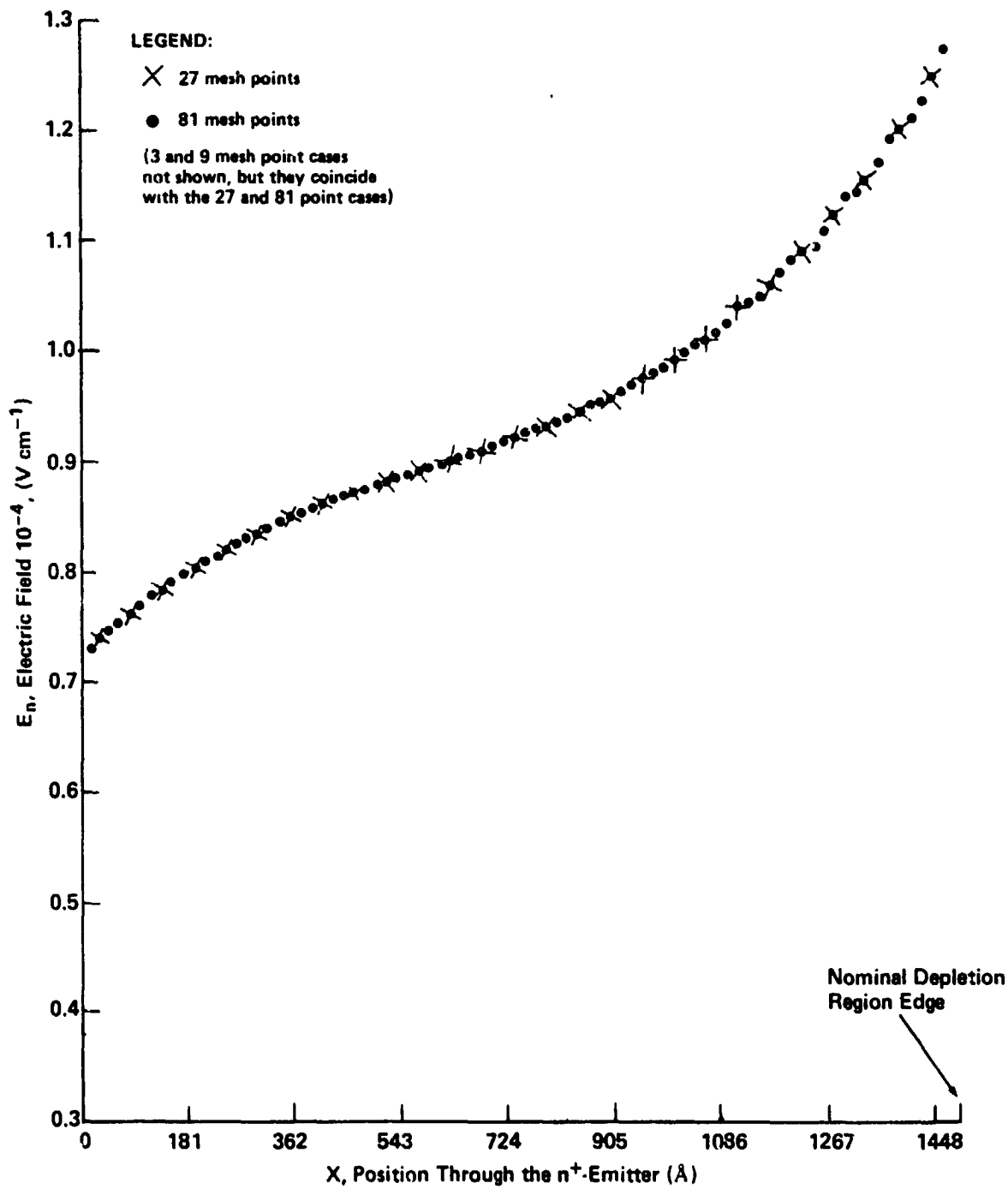


Figure 5. Built-in electric field vs. position in the n^+ -emitter of a solar cell using 27 and 81 mesh points under short-circuit current conditions and for three iterations per mesh point.

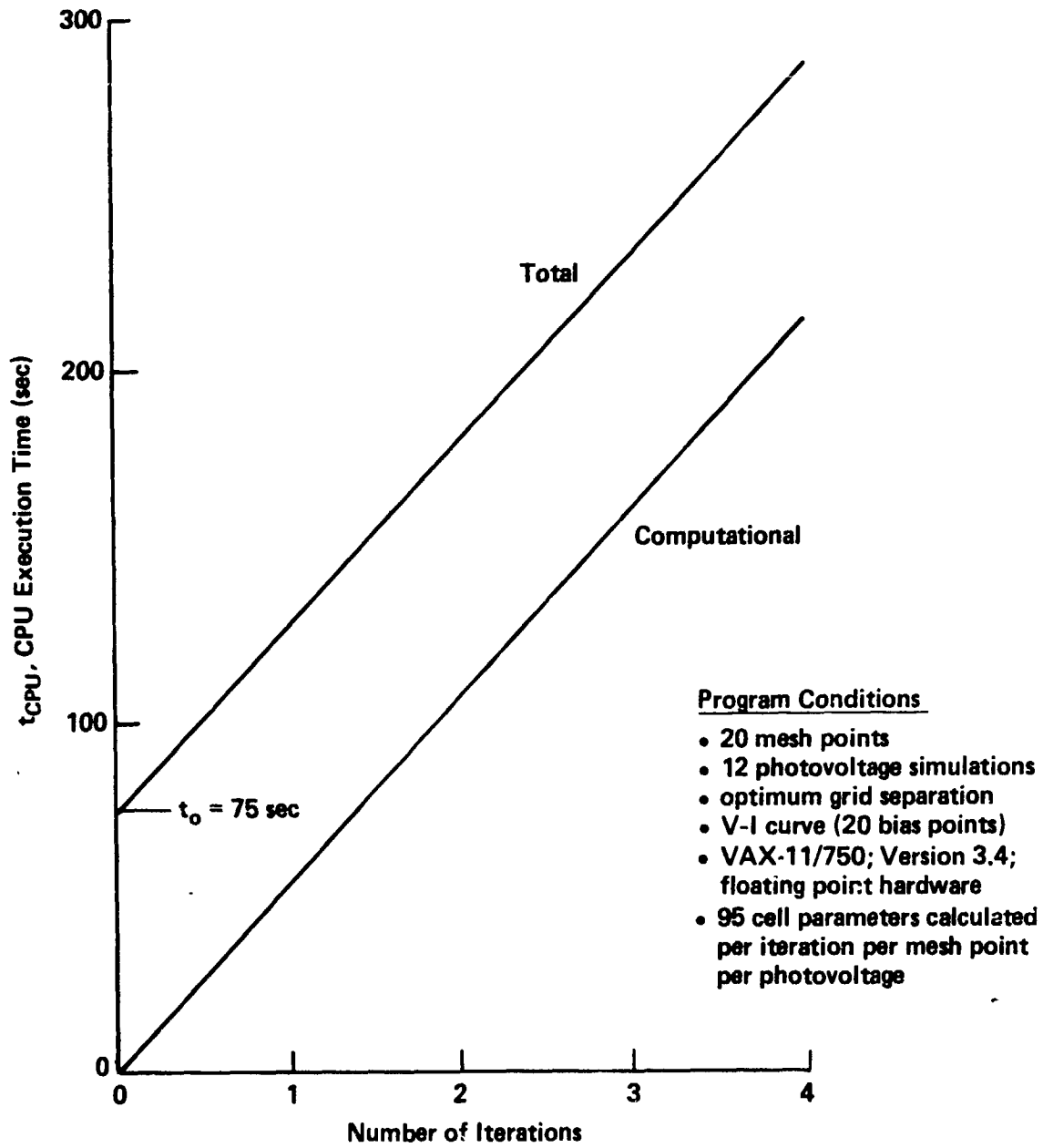


Figure 6. CPU execution time vs. number of iterations using 20 mesh points and 12 photovoltage simulations.



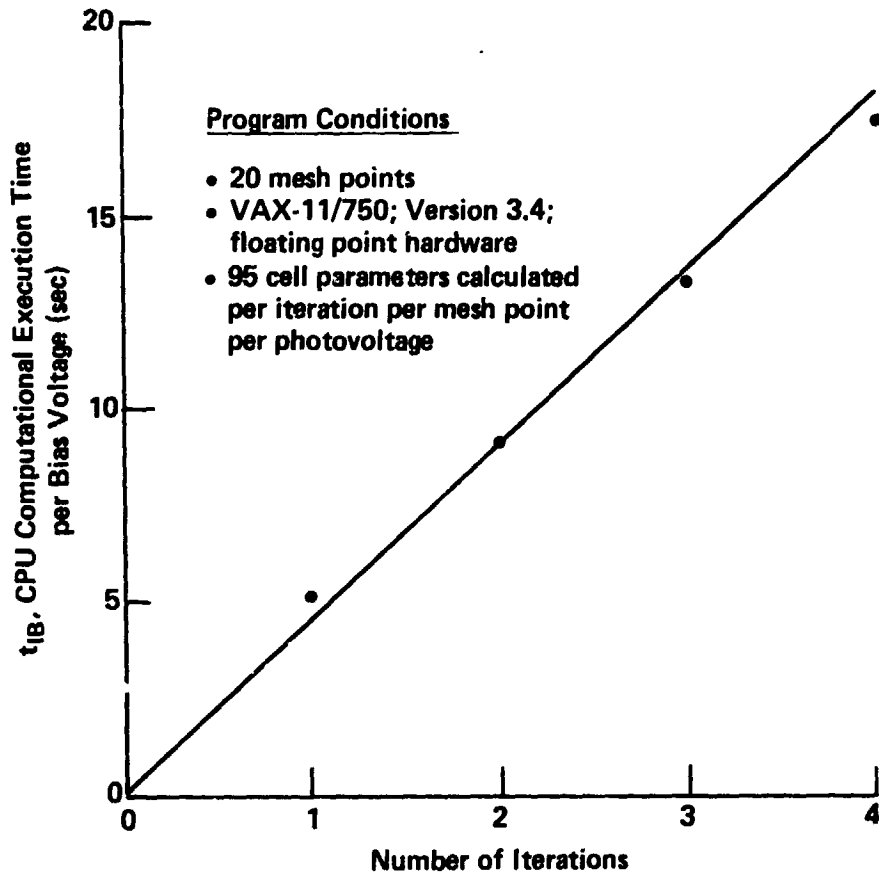


Figure 7. CPU computational time per photovoltage vs. number of iterations per mesh point using 20 mesh points.

HIGH-EFFICIENCY DEVICE RESEARCH

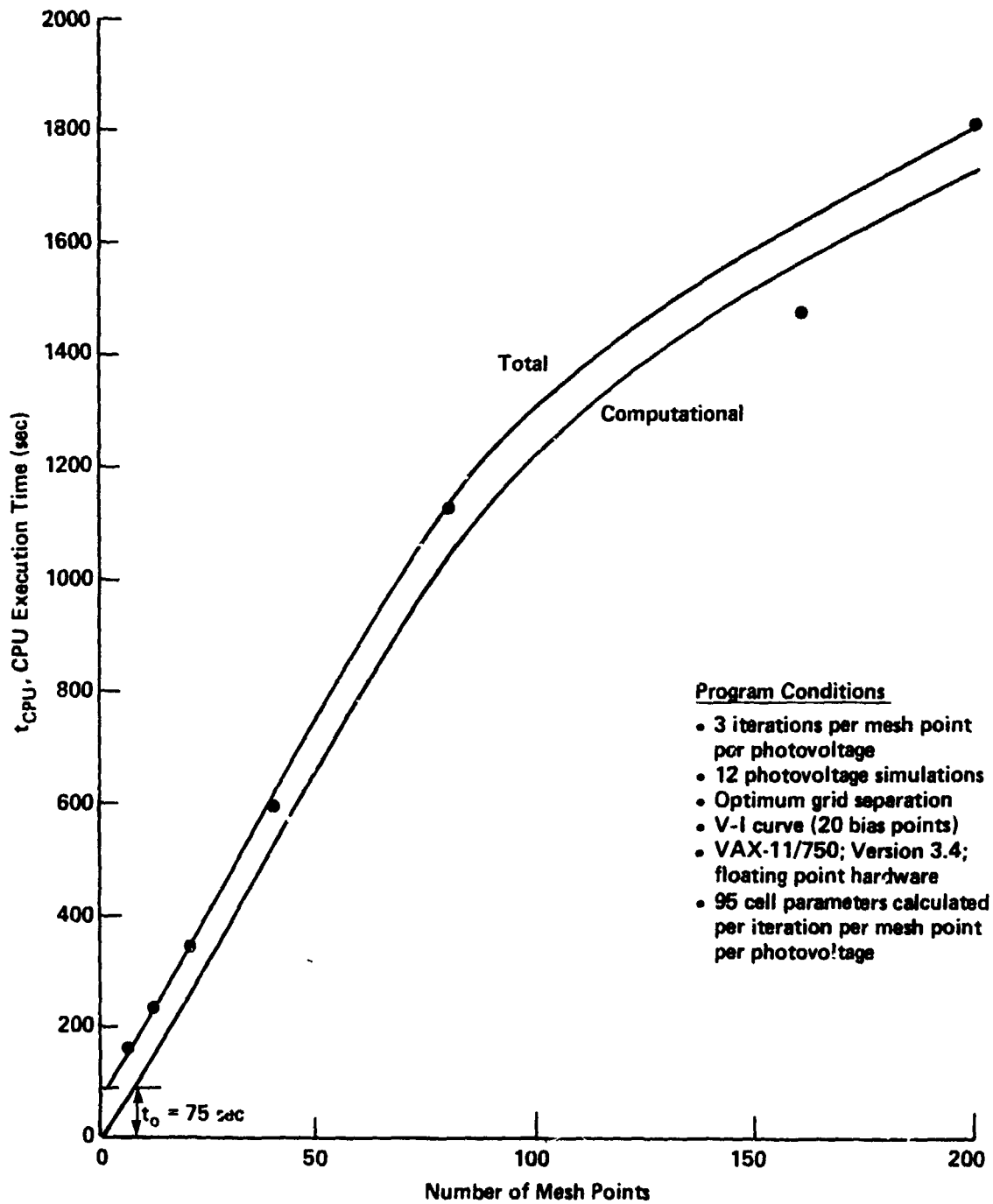


Figure 8. CPU execution time vs. number of mesh points using three iterations per mesh point and 12 photovoltage simulations.



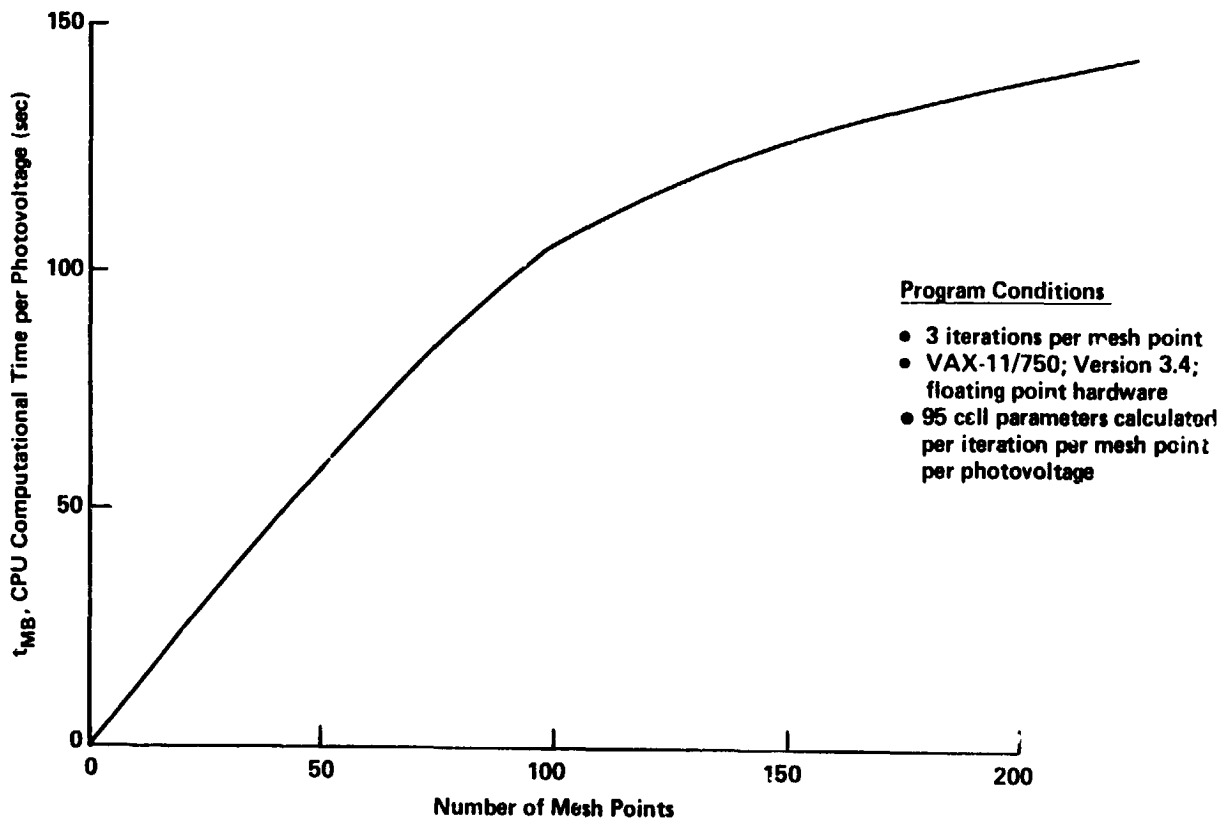


Figure 9. CPU computational time per photovoltage vs. number of mesh points using three iterations per mesh point.

HIGH-EFFICIENCY DEVICE RESEARCH

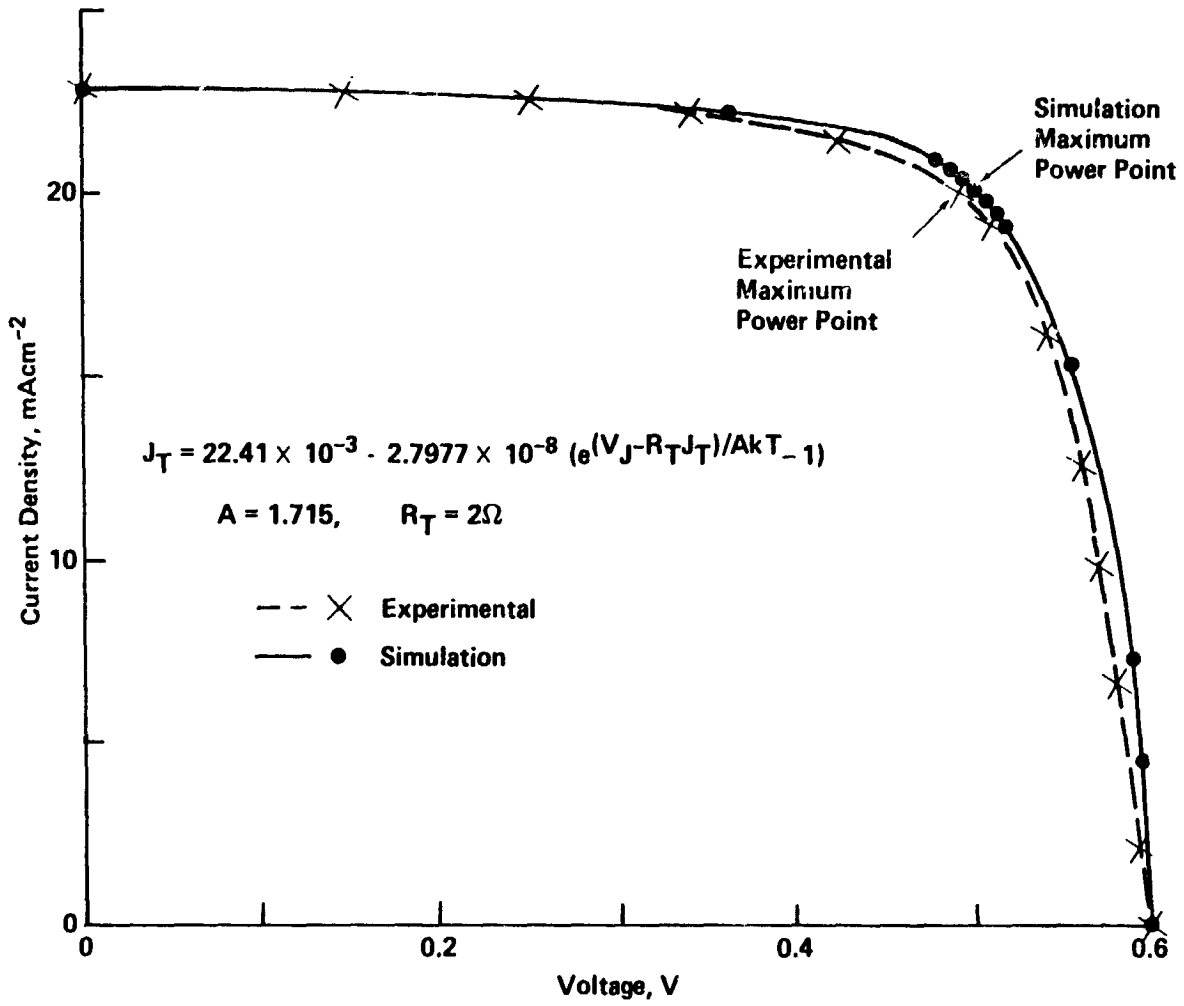


Figure 10. Simulated and experimentally determined V-I curve for cell No. 24C at 300 K, and the simulated diode equation.

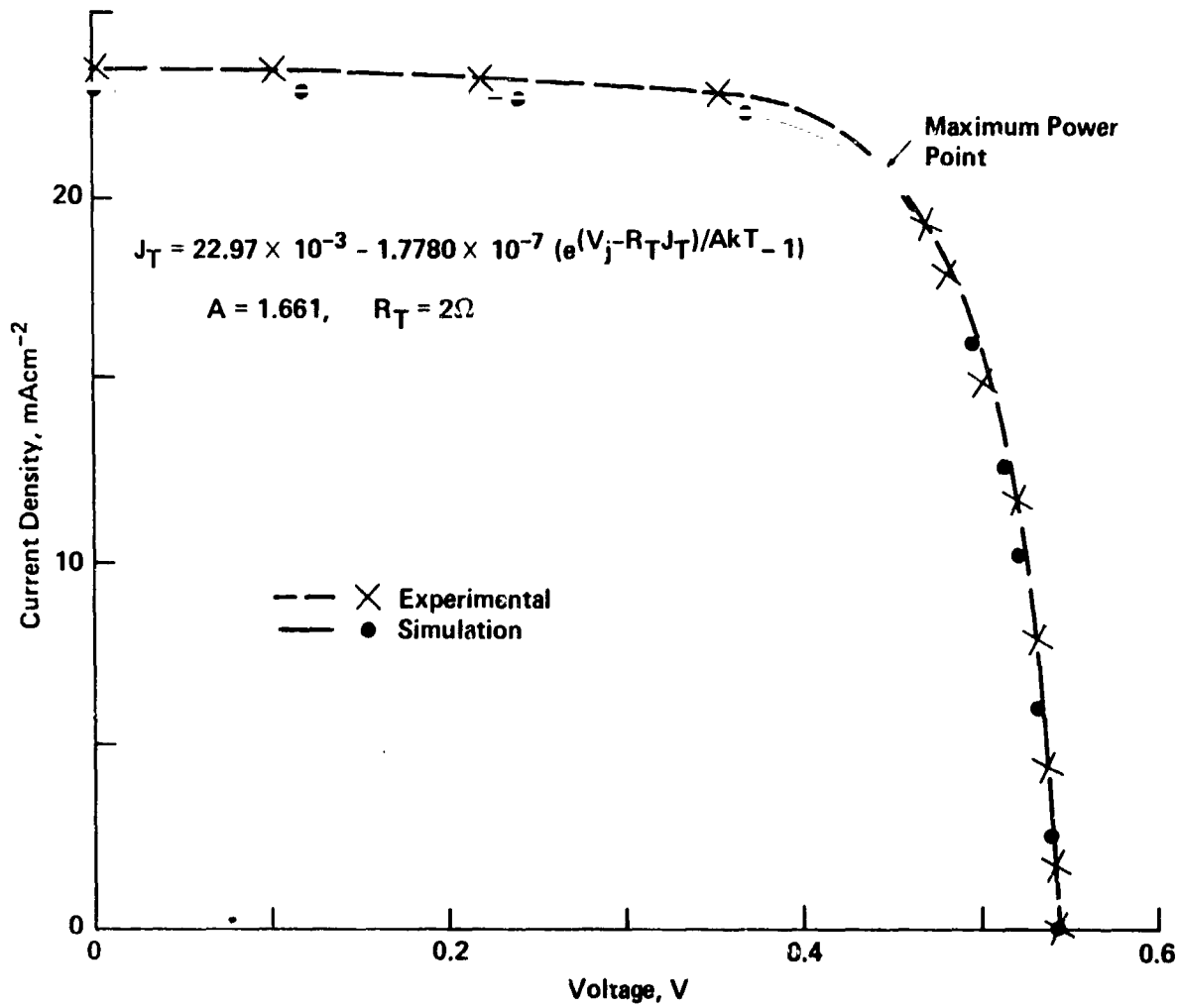


Figure 11. Simulated and experimentally determined V-I curve for cell No. 24C at 326 K and the diode equation obtained from the simulation program.

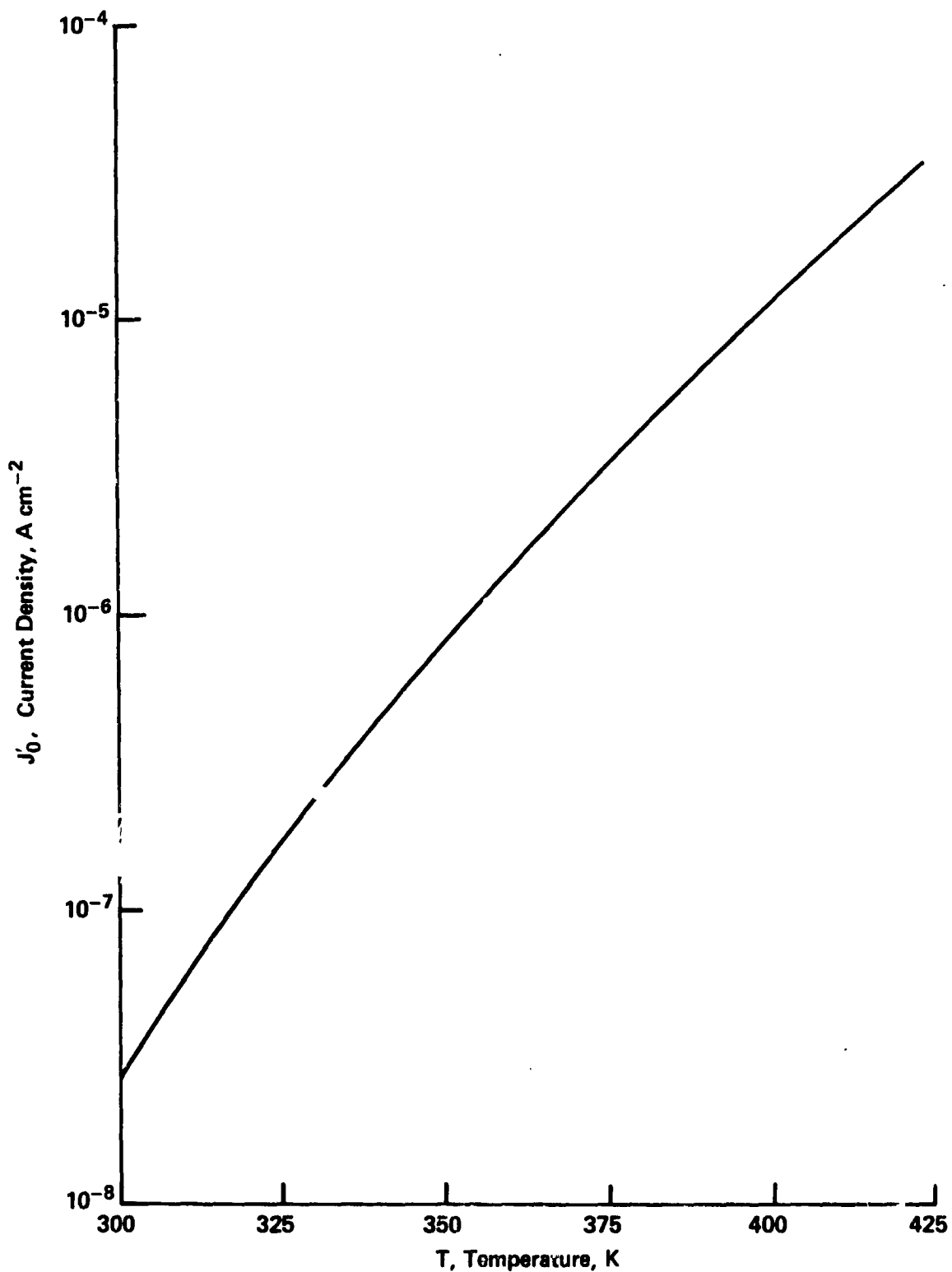


Figure 12. Equivalent saturation current density vs. temperature for cell No. 24C, obtained from simulation results.

HIGH-EFFICIENCY DEVICE RESEARCH

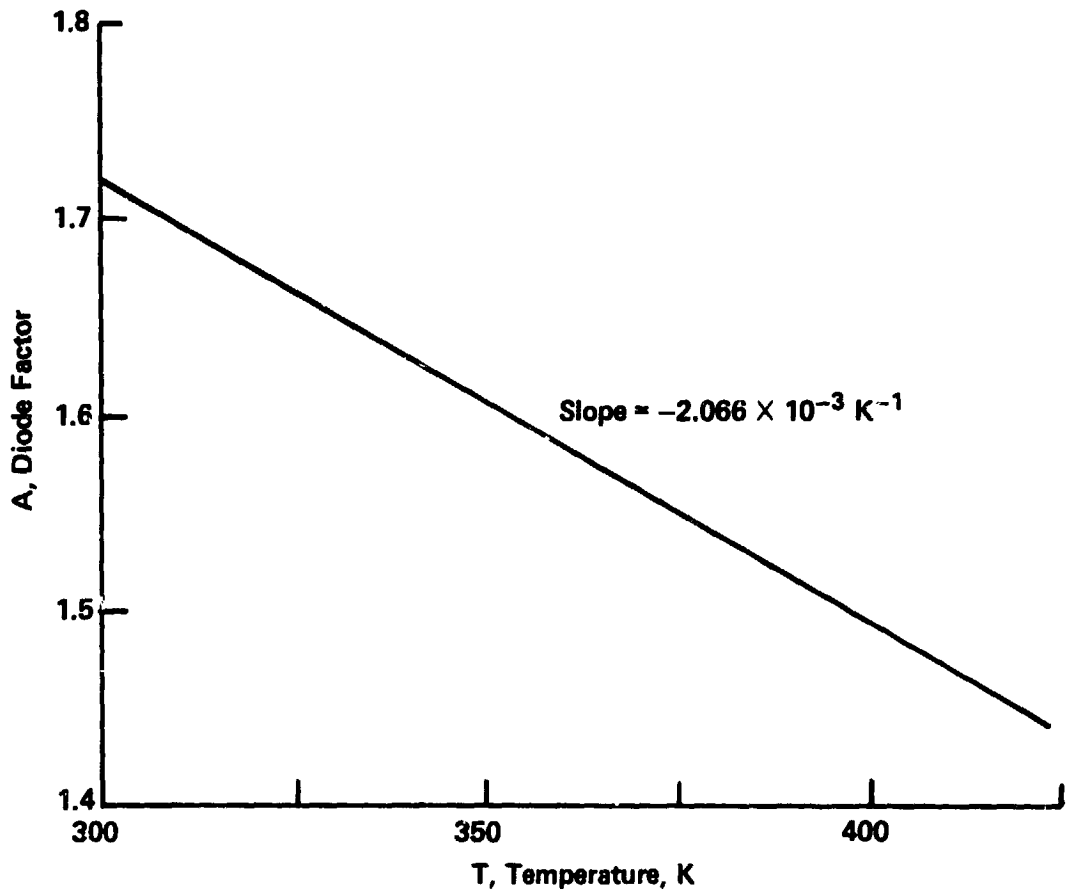


Figure 13. Diode factor vs. temperature for cell No. 24C, obtained from simulation results.



HIGH-EFFICIENCY DEVICE RESEARCH

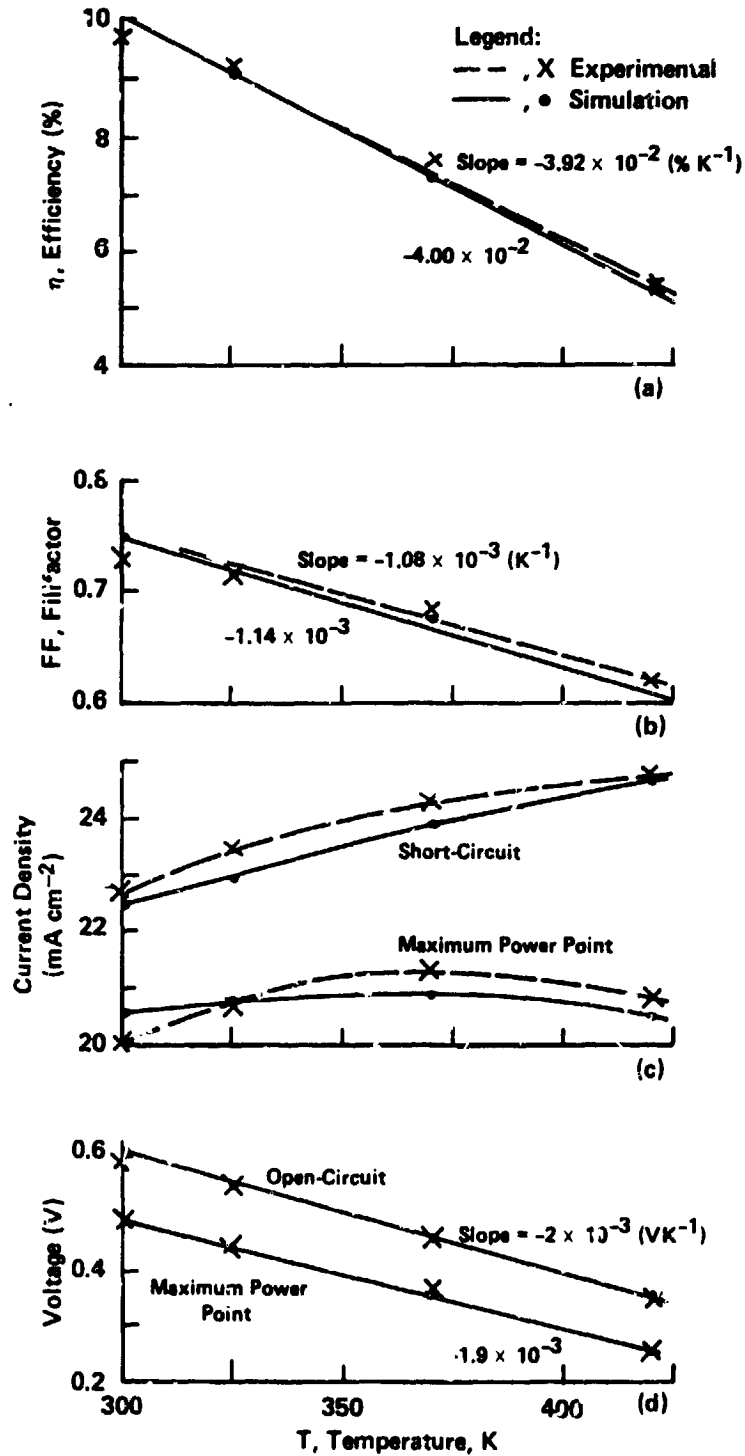


Figure 14. Simulation and experimental behavior of device terminal characteristics are presented over the temperature range of 300 to 421 K for solar cell No. 24C. Temperature coefficients represented by corresponding slopes are also shown where the slope is uniquely defined.



HIGH-EFFICIENCY DEVICE RESEARCH

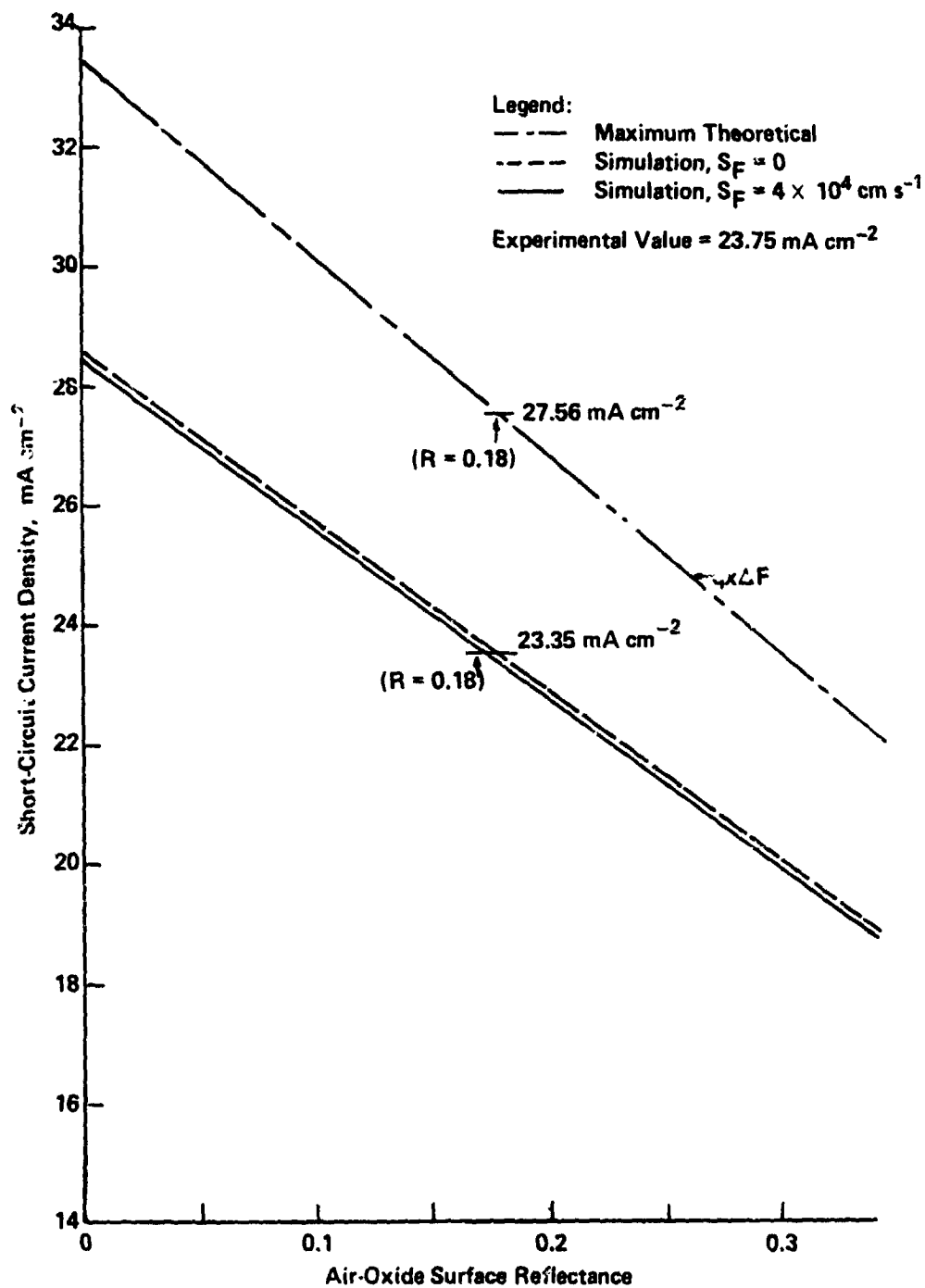


Figure 15. Maximum theoretical and simulation values of short-circuit current density vs. air-oxide reflectivity for cell No. 24C where shadowing correction is not made. Maximum theoretical current is calculated independently of the model and is based only on the absorbed photon flux and assuming 100-percent collection efficiency.

C-5

HIGH-EFFICIENCY DEVICE RESEARCH

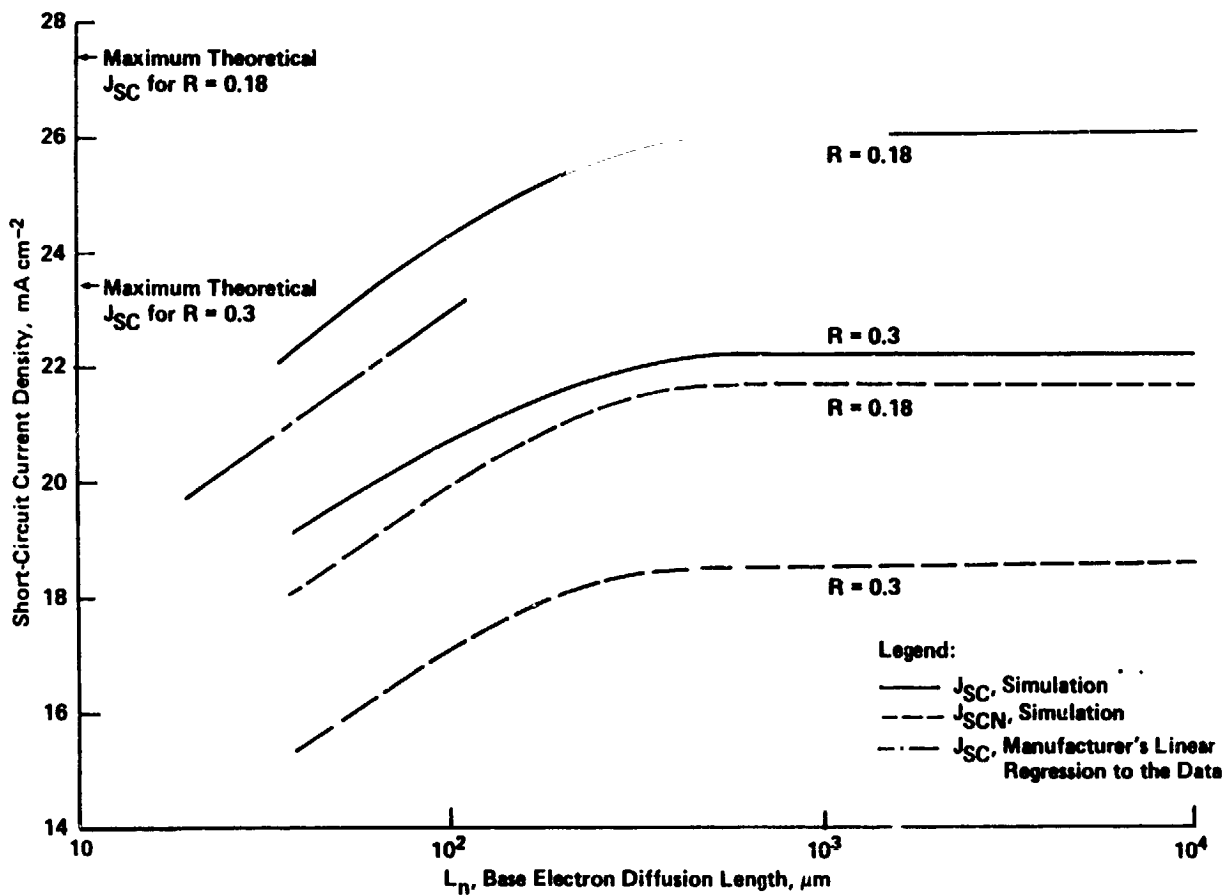


Figure 16. Simulation of total and base region electron contribution to short-circuit current density and linear regression to experimental data at 300 K. Maximum theoretical current is calculated independently of the model and is based only on the absorbed photon flux and assuming 100 percent collection efficiency.

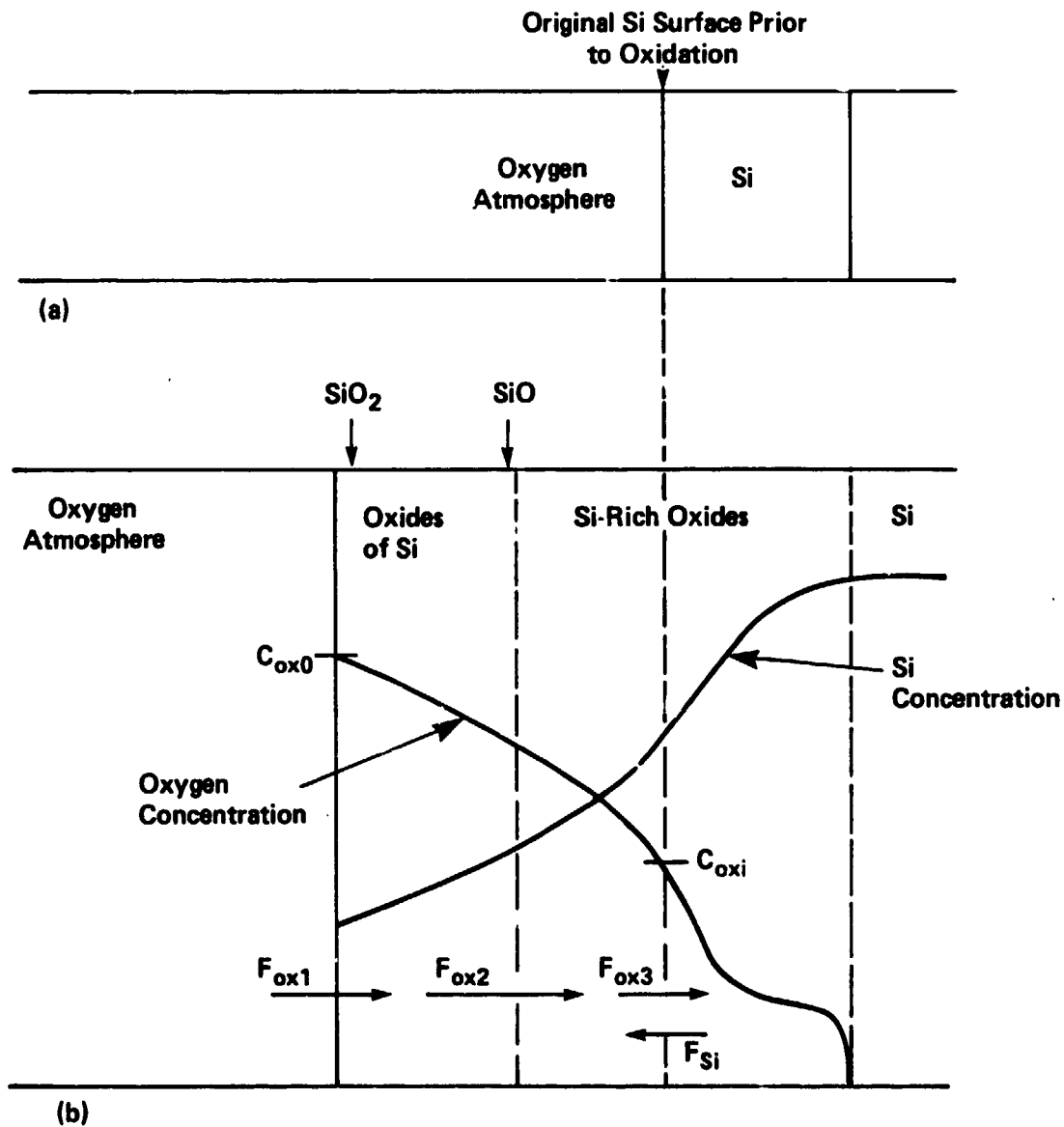


Figure 17. One-dimensional model representing the thermally grown Si-rich oxides: (a) prior to oxidation; and (b) during oxidation.

HIGH-EFFICIENCY DEVICE RESEARCH

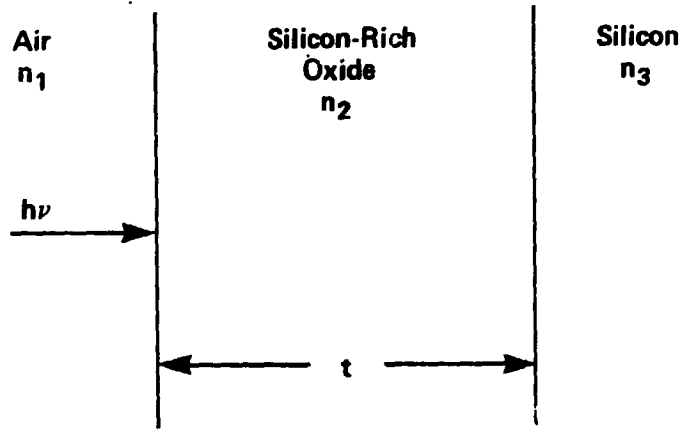


Figure 18. Model of thin film oxide on silicon under normal incidence.

HIGH-EFFICIENCY DEVICE RESEARCH

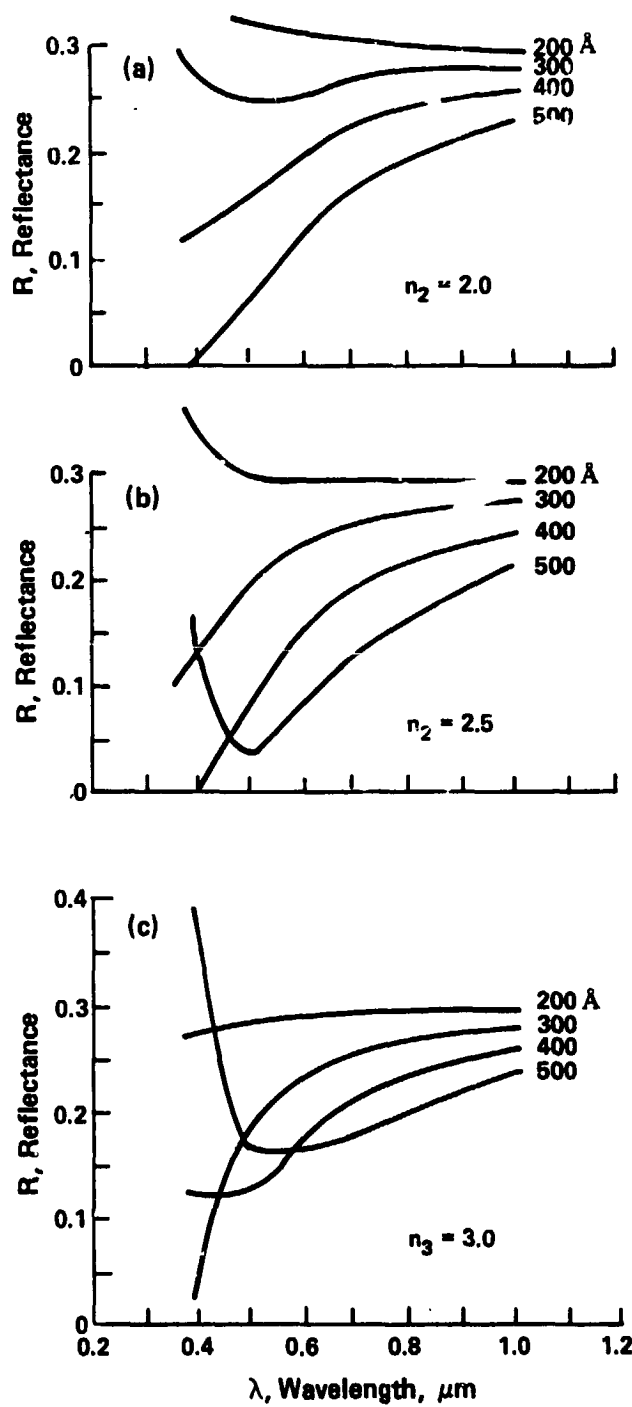


Figure 19. Reflectance under normal incidence at the air-oxide interface vs. wavelength for refractive indices representing silicon-rich oxides: (a) 2.0; (b) 2.5; and (c) 3.0. Oxide thickness is a parameter.

HIGH-EFFICIENCY DEVICE RESEARCH

Table 2. Photoexcited hole concentrations, their derivatives, and the percent differences in an n^+ -emitter region at three points (A, B, and C), for four mesh point distributions (3, 9, 27, 81) using three iterations at each mesh point.

Location	I, Emitter Mesh Points	P_{net} cm^{-3}	$\frac{dP_{net}}{dx}$ cm^{-4}	$\frac{P_{net} - P_{net(i)}}{P_{net(i)}} \times 10^2$ %	$\frac{\frac{dP_{net}}{dx} - \frac{dP_{net(i)}}{dx}}{\frac{dP_{net(i)}}{dx}} \times 10^2$ %
A = 245 Å	3	$P_{ne1} = 4.9185 \times 10^{10}$	7.4080×10^{15}	+10.1	+47.3
	9	$P_{ne2} = 4.6128 \times 10^{10}$	5.5105×10^{15}	+3.3	+5.6
	27	$P_{ne5} = 4.5050 \times 10^{10}$	5.0746×10^{15}	+0.9	+0.9
	81	$P_{ne(14)} = 4.4670 \times 10^{10}$	5.0286×10^{15}	—	—
A = 734 Å	3	$P_{ne2} = 5.2937 \times 10^{10}$	-3.8439×10^{15}	+2.8	-36.4
	9	$P_{ne5} = 5.2697 \times 10^{10}$	-3.0244×10^{15}	+2.3	-7.3
	27	$P_{ne(14)} = 5.1820 \times 10^{10}$	-2.8725×10^{15}	+0.6	-1.9
	81	$P_{ne(41)} = 5.1504 \times 10^{10}$	-2.8181×10^{15}	—	—
A = 1223 Å	3	$P_{ne3} = 2.6325 \times 10^{10}$	-6.9382×10^{15}	+16.9	+11.7
	9	$P_{ne6} = 2.3454 \times 10^{10}$	-7.8405×10^{15}	+3.0	+0.3
	27	$P_{ne(23)} = 2.2880 \times 10^{10}$	-7.8819×10^{15}	+0.5	-0.3
	81	$P_{ne(88)} = 2.2772 \times 10^{10}$	-7.8618×10^{15}	—	—

HIGH-EFFICIENCY DEVICE RESEARCH

Table 3. Parameters used in the simulation were provided by or deduced from manufacturers' specifications for cell No. 24C.

Cell Type	n ⁺ p
Total cell thickness	3.8×10^{-2} cm
Junction depth	1.8×10^{-5} cm
Contact shadowing	4 percent
Front surface concentration	4×10^{19} cm ⁻³
Front surface profile	erfc
Back surface concentration	0
Front SRV	4×10^4 cm S ⁻¹
Back SRV	3×10^3
Base region acceptor concentration	1.2×10^{17} cm ⁻³
Base electron diffusion length (at 300 K)	59×10^{-4} cm
n-Type dopant	Arsenic
Recombination trap level in n-region (As)	0.049 eV
p-Type dopant	Boron
Recombination trap level in p-region (B)	0.045 eV
Recombination concentration constant in p-region	1×10^{14} cm ⁻³
Recombination concentration constant in n-region	9.195×10^{12} cm ⁻³
Thickness of SiO ₂ passivation layer	50 to 200 Å
Air-oxide reflectivity (not provided by manufacturer)	0 to 0.34
Diode Resistance*	2 Ω
Temperature*	300 K 326 K 371 K 421 K

*Measured by RTI.

HIGH-EFFICIENCY DEVICE RESEARCH

Table 4(a).

Parameter	Simulation	Manufacturer		RTI/NC A&T	
		Data	% Diff	Data	% Diff
η , %	10.12	10.1	-0.2	9.8	-3.3
FF	0.749	0.74	-1.2	0.73	-2.6
J_{sc} , mA cm ⁻²	22.41	22.80	1.7	22.70	1.3
V_{oc} , V	0.6029	0.595	-1.3	0.5956	-1.2
J_{mp} , mA cm ⁻²	20.58	—	—	20.00	-2.9
V_{mp} , V	0.4918	—	—	0.4922	0.08

Table 4(b).

Parameter	Simulation	RTI/NC A&T	% Difference
η , %	9.1	9.3	2.2
FF	0.724	0.723	-0.1
J_{sc} , mA cm ⁻²	22.97	23.45	2.1
V_{oc} , V	0.5493	0.5458	-0.6
J_{mp} , mA cm ⁻²	20.79	20.71	-0.4
V_{mp} , V	0.4394	0.4462	1.5

Table 4(c).

Parameter	Simulation	RTI/NC A&T	% Difference
η , %	7.33	7.6	3.6
FF	0.674	0.687	1.9
J_{sc} , mA cm ⁻²	23.83	24.28	1.8
V_{oc} , V	0.4564	0.4558	-0.2
J_{mp} , mA cm ⁻²	20.85	21.37	2.5
V_{mp} , V	0.3518	0.3561	1.2

Table 4(d).

Parameter	Simulation	RTI/NC A&T	% Difference
η , %	5.29	5.4	2.04
FF	0.609	0.62	1.77
J_{sc} , mA cm ⁻²	24.63	24.78	0.67
V_{oc} , V	0.3525	0.3522	-0.10
J_{mp} , mA cm ⁻²	20.41	20.85	2.10
V_{mp} , V	0.2592	0.258	-0.70

Table 4. Results of validation study using cell No. 24C, with corresponding parameters listed in Table 3, and where 0.18 is used for the air-oxide reflectivity: a) 300 K; b) 326 K; c) 371 K; and d) 421 K. Simulation results are obtained using three iterations and 20 mesh points equally separated in the n- and p-regions.

HIGH-EFFICIENCY DEVICE RESEARCH

Table 5. Simulation and experimental temperature coefficients and the percent difference for cell No. 24C.

Temperature Coefficient	Simulation	Experimental	Percent Difference
$d\eta/dT, (\% K^{-1})$	-4.00×10^{-2}	-3.92×10^{-2}	-2.04
$d(FF)/dT, (K^{-1})$	-1.14×10^{-3}	-1.08×10^{-3}	-5.90
$dV_{oc}/dT, (VK^{-1})$	-2.10×10^{-3}	-2.04×10^{-3}	-2.90
$dV_{mp}/dT, (VK^{-1})$	-1.93×10^{-3}	-1.94×10^{-3}	0.52

Table 6. Summary of experimental, calculated, and simulated short-circuit current density for cell No. 24C at 300 K.

Method	Short-circuit current density*	Reflectivity	Comments
Experimental	$23.75 \times 10^{-3} \text{ mA cm}^{-2}$	unknown	agreement with RTI data
Calculated (simulation program was not used)	$18.50 \times 10^{-3} \text{ mA cm}^{-2}$	unknown	using manufacturer's spectral response curve and the revised AM1.5 spectral data
Calculated (simulated program was not used)	$22.90 \times 10^{-3} \text{ mA cm}^{-2}$	0.32	maximum theoretical value by calculating absorbed flux and assuming 100% collection efficiency
	$27.56 \times 10^{-3} \text{ mA cm}^{-2}$	0.18	
Simulation Results	$23.35 \times 10^{-3} \text{ mA cm}^{-2}$	0.18	RTI simulation program used (resultant collection efficiency is approximately 85%)

*Uncorrected for contact shadowing.